

# A Methodology of Fabricating Novel Electrodes for Semiconductor Devices: Doping and Van der Waals Integrating Organic Semiconductor Films

Ping-An Chen, Junjun Guo, Xinwen Yan, Yu Liu, Huan Wei, Xincan Qiu, Jiangnan Xia, Jing Guo, Jiaqi Ding, Zhenqi Gong, Chen Chen, Ting Lei, Huajie Chen,\* Zebing Zeng,\* and Yuanyuan Hu\*

Electrodes are indispensable components in semiconductor devices, and now are mainly made from metals, which are convenient for use but not ideal for emerging technologies such as bioelectronics, flexible electronics, or transparent electronics. Here the methodology of fabricating novel electrodes for semiconductor devices using organic semiconductors (OSCs) is proposed and demonstrated. It is shown that polymer semiconductors can be heavily p- or n-doped to achieve sufficiently high conductivity for electrodes. In contrast with metals, the doped OSC films (DOSCFs) are solution-processable, mechanically flexible, and have interesting optoelectronic properties. By integrating the DOSCFs with semiconductors through van der Waals contacts different kinds of semiconductor devices can be constructed. Importantly, these devices exhibit higher performance than their counterparts with metal electrodes, and/or excellent mechanical or optical properties that are unavailable in metal-electrode devices, suggesting the superiority of DOSCF electrodes. Given the existing large amount of OSCs, the established methodology can provide abundant electrode choices to meet the demand of various emerging devices.

## 1. Introduction


Semiconductor devices such as diodes, transistors, etc. are core building blocks for various electronic circuits and products.<sup>[1–6]</sup> Generally, semiconductor devices are composed of semiconductors as active layers, metals as electrodes and insulators as dielectrics. Although semiconductor layer is arguably the most important component in semiconductor devices, electrodes also play fundamental role in determining device performance. However, compared to the great developments in semiconductors, the electrodes, which have been mostly made of metals such as gold (Au), silver (Ag), or copper (Cu), experience less significant progress. With the emergence of novel devices and technologies, metal electrodes are facing difficulties and challenges. For instance, metal electrodes are inappropriate for

P.-A. Chen, Y. Liu, H. Wei, X. Qiu, J. Xia, J. Guo, J. Ding, Z. Gong, Y. Hu  
International Science and Technology Innovation Cooperation Base  
for Advanced Display Technologies of Hunan Province  
School of Physics and Electronics  
Hunan University  
Changsha 410082, P. R. China  
E-mail: yhu@hnu.edu.cn

P.-A. Chen, Y. Liu, H. Wei, X. Qiu, J. Xia, Y. Hu  
Shenzhen Research Institute of Hunan University  
Shenzhen 518063, P. R. China

P.-A. Chen, Y. Hu  
Changsha Semiconductor Technology and Application Innovation  
Research Institute  
College of Semiconductors (College of Integrated Circuits)  
Hunan University  
Changsha 410082, P. R. China

J. Guo  
Institute of Functional Nano & Soft Materials (FUNSOM) Jiangsu  
Key Laboratory for Carbon-Based Functional Materials and Devices  
Soochow University  
Suzhou 215123, P. R. China

 The ORCID identification number(s) for the author(s) of this article can be found under <https://doi.org/10.1002/smll.202207858>.

X. Yan, T. Lei  
Key Laboratory of Polymer Chemistry and Physics of Ministry of  
Education  
School of Materials Science and Engineering  
Peking University  
Beijing 100871, P. R. China

C. Chen  
Science and Technology on Advanced Ceramic Fibers and Composites  
Laboratory  
College of Aerospace Science and Engineering  
National University of Defense Technology  
Changsha 410000, P. R. China

H. Chen  
Key Laboratory of Environmentally Friendly Chemistry and Applications  
of Ministry of Education  
College of Chemistry  
Xiangtan University  
Xiangtan 411105, P. R. China  
E-mail: chenjie@xtu.edu.cn

Z. Zeng  
State Key Laboratory of Chemo/Biosensing and Chemometrics  
College of Chemistry and Chemical Engineering  
Hunan University  
Changsha 410082, P. R. China  
E-mail: zbzeng@hnu.edu.cn

DOI: 10.1002/smll.202207858

realizing flexible/stretchable electronics because they are intrinsically brittle and rigid, although this problem can be partially addressed by rationally designed architectures including metal meshes and metal nanowires.<sup>[7–11]</sup> In addition, the processing of the metal electrodes usually requires high vacuum for thermal evaporation or electron-beam evaporation, which not only increases production cost, but also may cause damage to semiconductors due to thermal irradiation or metal atom bombardment, resulting in degradation of device performance.<sup>[12–14]</sup> Besides, metal electrodes are not good choices for bioelectronics, especially for implantable electronics due to their toxicity. Therefore, it is highly desirable to develop novel electrodes that can address the above-mentioned problems.

Within this background, conductive polymers (CPs) which are not only conductive but also have good mechanical properties and biocompatibility were reported as electrodes.<sup>[15–17]</sup> However, by far there have been only a few CPs available, which can hardly meet the requirements of various devices. As an example, PEDOT:PSS is the most frequently used CP with p-type conductivity and work function of  $\approx 4.7$  eV; it can only be used as electrodes for p-type semiconductors with valence band (VB) or highest occupied molecular orbital (HOMO) close to  $-4.7$  eV. Besides, by far there have been rare reports of n-type CPs as electrodes for n-type devices. Thus, the application of CPs as electrodes remains limited.

In contrast with the limited number of CPs, there are hundreds or thousands of organic semiconductors (OSCs) which can also be processed by low-temperature solution-process and intrinsically possess mechanical flexibility, stretchability and biocompatibility.<sup>[18,19]</sup> In particular, the abundance and diversity of OSCs in electrical properties such as energy levels, polarity, and optical properties offer enormous choices to match the requirement of semiconductor devices, making them very attractive for electrodes. However, the intrinsic conductivity of OSCs is generally less than  $10^{-2}$  S cm<sup>-1</sup>, which prevents them from being conductive electrodes. With the development of doping techniques for OSCs, the conductivity of OSCs can be elevated to values comparable to that of metals ( $100\text{--}1000$  S cm<sup>-1</sup>) by proper doping.<sup>[20–22]</sup> All these facts suggest that OSC films have great potential to be developed as novel electrodes for semiconductor devices, yet the corresponding methodology is still in lack.

In this study, we demonstrate the methodology of doping and integrating OSC films for electrodes of semiconductor devices and show the advantages of doped OSC film (DOSCF) electrodes over conventional metal electrodes. As an example, we show the p-doped PBBT-2T films can reach conductivity of more than  $120$  S cm<sup>-1</sup> and work function of  $-5.3$  eV. The PBBT-2T DOSCFs have smooth morphology, and meanwhile are stretchable and semi-transparent, which are distinct properties absent in metals. We then employ polydimethylsiloxane (PDMS) stamping transfer method to transfer the DOSCFs onto semiconductor layers, forming van der Waals (vdW) contacts. Various kinds of devices such as field-effect transistors (FETs) and photodiodes (PDs) based on different semiconductors are successfully fabricated with DOSCFs as electrodes. Remarkably, the DOSCF devices not only possess high electrical performance, but also exhibit excellent mechanical or optical properties that are unavailable in metal-electrode

devices. Moreover, we present that the proposed methodology is not only applicable to PBBT-2T, but can be extended to other p- or n-type OSCs. Finally, we showcase the proof-of-concept all-organic FETs, which are available thanks to the availability of DOSCF electrodes. This work not only provides a methodology to obtain many different electrodes, but also opens up new opportunities for developing devices with novel functions.

## 2. Results and Discussion

### 2.1. Doping and Characterization of PBBT-2T Films

To be eligible for electrodes, the DOSCFs need to be sufficiently conductive. In addition, uniform film morphology with low roughness is also demanded for forming a close contact with semiconductors, which is critical for efficient charge injection/extraction. Fortunately, the recent developments in OSCs and dopants provide us chances to achieve such DOSCFs. In this study, we used a benzobisthiadiazole (BBT)-based D-A copolymer PBBT-2T as the host p-type semiconductor (see **Figure 1a**), and a highly efficient p-dopant trityl tetrakis(pentafluorophenyl) borate (TrTPFB) which can significantly enhance the conductivity of various semiconductors with little disruption to the film structure/morphology as the dopant.<sup>[23–27]</sup>

To characterize the electrical properties of PBBT-2T, bottom-gate top-contact (BGTC) devices with Au electrodes were fabricated, whose transfer and output characteristics are illustrated in **Figure 1b,c**, respectively. These results show PBBT-2T is a p-type semiconductor with hole mobility of  $\approx 0.1$  cm<sup>2</sup> V<sup>-1</sup> s<sup>-1</sup>. In order to see if PBBT-2T can be effectively doped by TrTPFB, UV-vis-NIR absorption spectra was employed to characterize the doped semiconductor solutions. **Figure 1d** shows the pristine PBBT-2T exhibits two main absorption peaks at  $\approx 504$  and  $1140$  nm. As the polymer is doped with TrTPFB, the low-energy broad absorption in the near-infrared region (above  $1500$  nm) appears, and this absorption gets stronger as the doping concentration increases. These new spectral features are attributed to doping-induced polarons and can be considered as proof that doping occurs in the polymer.

In addition to UV-vis-NIR spectroscopy, electron spin resonance (ESR) measurements were performed at room temperature. As shown in **Figure 1e**, strong paramagnetic signals for  $1$  mol% TrTPFB-doped PBBT-2T polymer could be observed, suggesting the existence of unpaired electrons when TrTPFB was blended with PBBT-2T. These results unambiguously confirm that doping occurs when TrTPFB is blended with PBBT-2T.

To evaluate the possibility of using the DOSCFs for electrodes, we firstly measured electrical conductivity ( $\sigma$ ) (**Figure S1**, Supporting Information). **Figure 1f** shows the electrical conductivity of the pristine and doped PBBT-2T thin films at different doping levels. The pristine PBBT-2T films show low  $\sigma$  of  $1.2 \times 10^{-2}$  S cm<sup>-1</sup>. Upon doping by TrTPFB, the doped PBBT-2T films show significant conductivity increase and reach the highest  $\sigma$  average of  $1.2 \times 10^2$  S cm<sup>-1</sup> at a doping concentration of  $30\text{--}40$  mol%. The dramatic increase of conductivity about four orders of magnitude in doped films suggests the excellent doping ability of TrTPFB, in consistent with previous reports.<sup>[25,26]</sup> However, further increasing the doping ratio leads

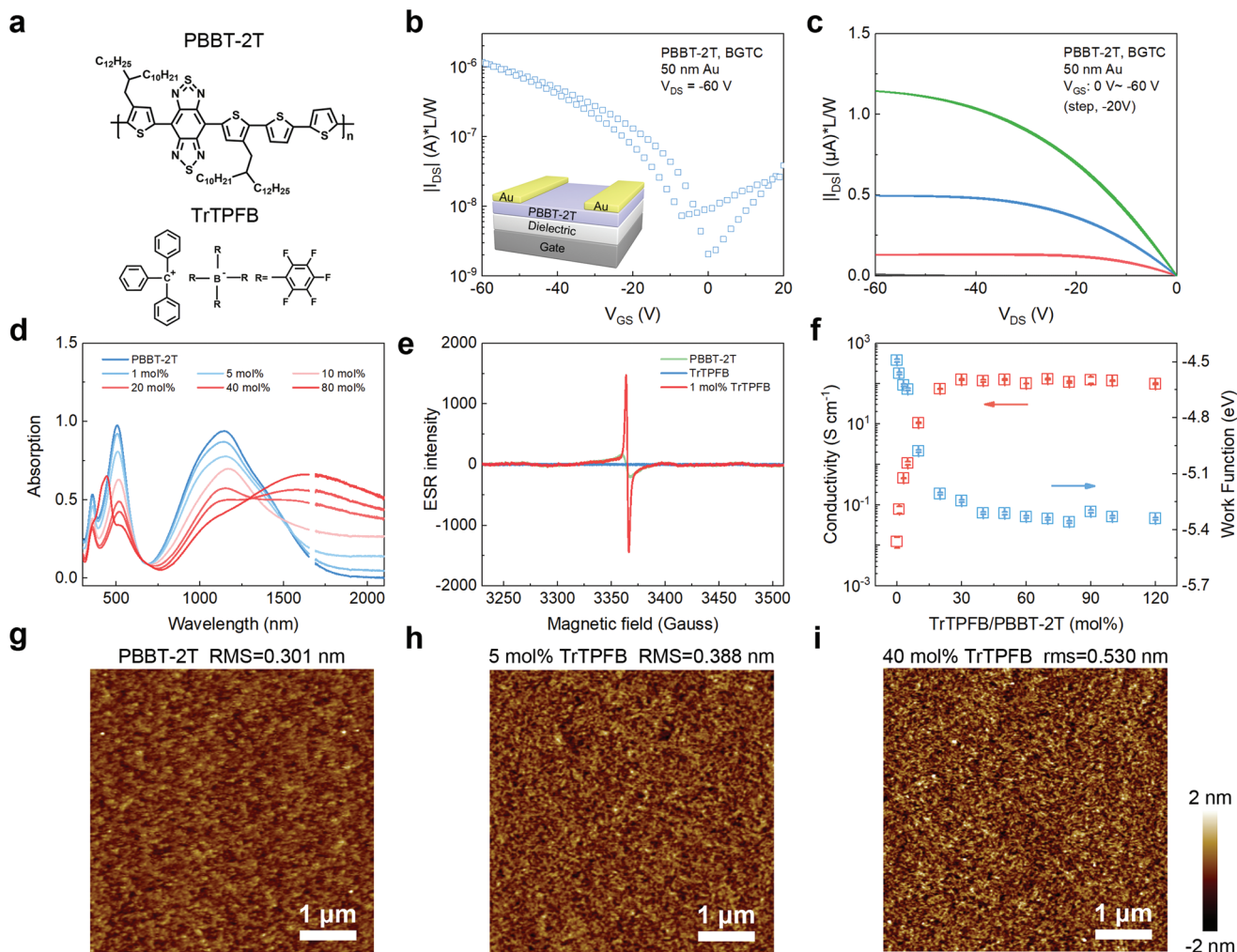


**Figure 1.** Characterization of the electrical and structural properties of doped PBBT-2T films. a) The molecule structures of polymer PBBT-2T and dopant TrTPFB. The transfer b) and output c) characteristics of pristine PBBT-2T FETs using BGTC device structure (channel length  $L = 150 \mu\text{m}$  and channel width  $W = 1000 \mu\text{m}$ ). d) the UV-vis-NIR absorption spectra of PBBT-2T and TrTPFB doped samples with varied molar ratio from 0 to 80 mol%. e) ESR spectra of pristine PBBT-2T, TrTPFB and 1 mol% doped sample. f) Conductivity and work function of doped PBBT-2T films as a function of dopant molar ratio. AFM images for g) pristine, h) 5 mol%, and i) 40 mol% TrTPFB/PBBT-2T films.

to slight decrease in electrical conductivities, probably due to the reduced connections between polymer chains and/or the disruption of polymer structure by dopants.

One may ask if the conductivity of the DOSCFs ( $> 100 \text{ S cm}^{-1}$ ) is high enough for electrodes of semiconductor devices. To answer this question, we estimated the required conductivity for electrodes of semiconductor devices such as organic field-effect transistors (OFETs) by considering that the conductivity of electrodes should provide enough current density for the devices. It turns out that for FETs based on semiconductors with mobility less than  $20 \text{ cm}^2 \text{ V}^{-1} \text{ s}^{-1}$  (e.g., OSCs or perovskite semiconductors), only a conductivity of  $\approx 10\text{--}100 \text{ S cm}^{-1}$  is needed (see Figure S2, Supporting Information). For other devices such as photodiodes or solar cells, further lower conductivity is required for electrodes since the current density in these devices is generally lower than that in FETs. Therefore, the conductivity of the PBBT-2T DOSCFs we obtained here is high enough for the usage as electrodes.

In addition, the work function of electrodes, which determines the Schottky barrier height of the contacts, is critical to the performance of devices. We thus characterized the work function of the PBBT-2T DOSCFs by Kelvin probe (Figure S1, Supporting Information). As shown in Figure 1f, the work function shifts from  $-4.5$  to  $-5.3 \text{ eV}$  as the doping level increases, being consistent with the occurrence of p-doping. The tunability of the work function of DOSCFs in a wide range by doping ratios is attractive since this allows good match with the energy levels of semiconductors.

Furthermore, atomic force microscopy (AFM) characterizations were carried out on undoped and doped films with different TrTPFB contents to investigate the influence of the dopant on the surface morphology of PBBT-2T films. As illustrated in Figure 1g, the morphology of pristine PBBT-2T films exhibits a very smooth surface with root-mean-square (RMS) of  $0.31 \text{ nm}$ . As TrTPFB is introduced into the films, the film morphology is hardly changed; the RMS value slightly increases

to 0.39 nm at doping of 5 mol%, and the RMS is as low as 0.53 nm (Figure 1h) even at the high doping ratio of 40 mol% (Figure 1i). Such high uniformity of the films not only guarantees the superior conductivity of the films, but also enables the formation of good electrical contacts with semiconductors.

## 2.2. General Applicability of DOSCFs as vdW Electrodes for FETs

To investigate the feasibility of using DOSCFs as electrodes for semiconductor devices, we first fabricated OFETs by employing PBBT-2T DOSCFs as source/drain electrodes. Although the DOSCFs can be easily processed by solution method, it cannot be directly deposited onto with OSC films since the layer underneath will be damaged due to solubility, which is the key challenge for integrating the DOSCFs with OSCs. Therefore, in this study we utilized the PDMS stamping transfer method for fabricating electrical contacts using DOSCFs, with the device fabrication process illustrated in Figure 2. Specifically, a PDMS stamp was prepared with predefined source/drain patterns (see the experimental section for more details), on which the doped PBBT-2T films (40 mol% TrTPFB) were deposited by spin-coating. Then, the DOSCFs with film thickness of  $\approx 90$  nm (Figure S4, Supporting Information) were transferred and released onto semiconductor films prepared on Si<sup>++</sup>/SiO<sub>2</sub> substrate to form vdW top-contacts. In this way, bottom-gate top-contact (BGTC) FETs were obtained.

Figure 3a presents the transfer characteristics of PDVT-10 FETs with PBBT-2T DOSCFs (40 mol% TrTPFB) as source/drain electrodes and the control devices with Au electrodes.

In contrast with the control device showing ambipolar transport and large hysteresis, the DOSCF device exhibits beautiful transfer characteristic with unipolar p-channel transport and little hysteresis. The output characteristics shown in Figure 3d for the DOSCF device also suggest the unipolar p-channel transport and small hysteresis of the DOSCF device. Data analysis indicates the DOSCF device exhibits average mobility of  $0.22 \text{ cm}^2 \text{ V}^{-1} \text{ s}^{-1}$  and subthreshold swing (SS) of  $1.55 \text{ V dec}^{-1}$ , in contrast with the Au-electrode device showing average mobility of  $0.10 \text{ cm}^2 \text{ V}^{-1} \text{ s}^{-1}$  and SS of  $2.98 \text{ V dec}^{-1}$  (see Figure 3g). The enhanced device performance in the DOSCF devices is probably due to the high work function ( $\approx -5.3 \text{ eV}$ ) and the hole-transport nature of DOSCFs, which can significantly inhibit electron transport and lower injection barriers for holes, rendering them particularly suitable for p-channel devices. Notably, we indeed fabricated devices using PBBT-2T DOSCFs with various doping levels, yet it turns out that the 40 mol% devices showed the best performance (Figures S5 and S6, Supporting Information).

Furthermore, we employed C8-BTBT, which has a deep HOMO of  $-5.7 \text{ eV}$ , for fabricating OFETs.<sup>[28,29]</sup> Single crystal (C8-BTBT) was grown using solvent vapor annealing method (SVA).<sup>[30,31]</sup> DOSCF devices and control devices with Au electrodes were obtained following the above procedures (Figure S8, Supporting Information). The Au-electrode device shows poor performance in terms of large  $V_{\text{TH}}$  ( $-35 \text{ V}$ ) and SS ( $5.27 \text{ V dec}^{-1}$ ), which is possibly accounted by two reasons: 1) There is significant Schottky barrier at the electrode/semiconductor interface caused by the energy difference ( $\approx 0.6 \text{ eV}$ ) between the Fermi level of Au and HOMO of C8-BTBT. 2) There are interface traps because the bombardment of Au atoms during evaporation will

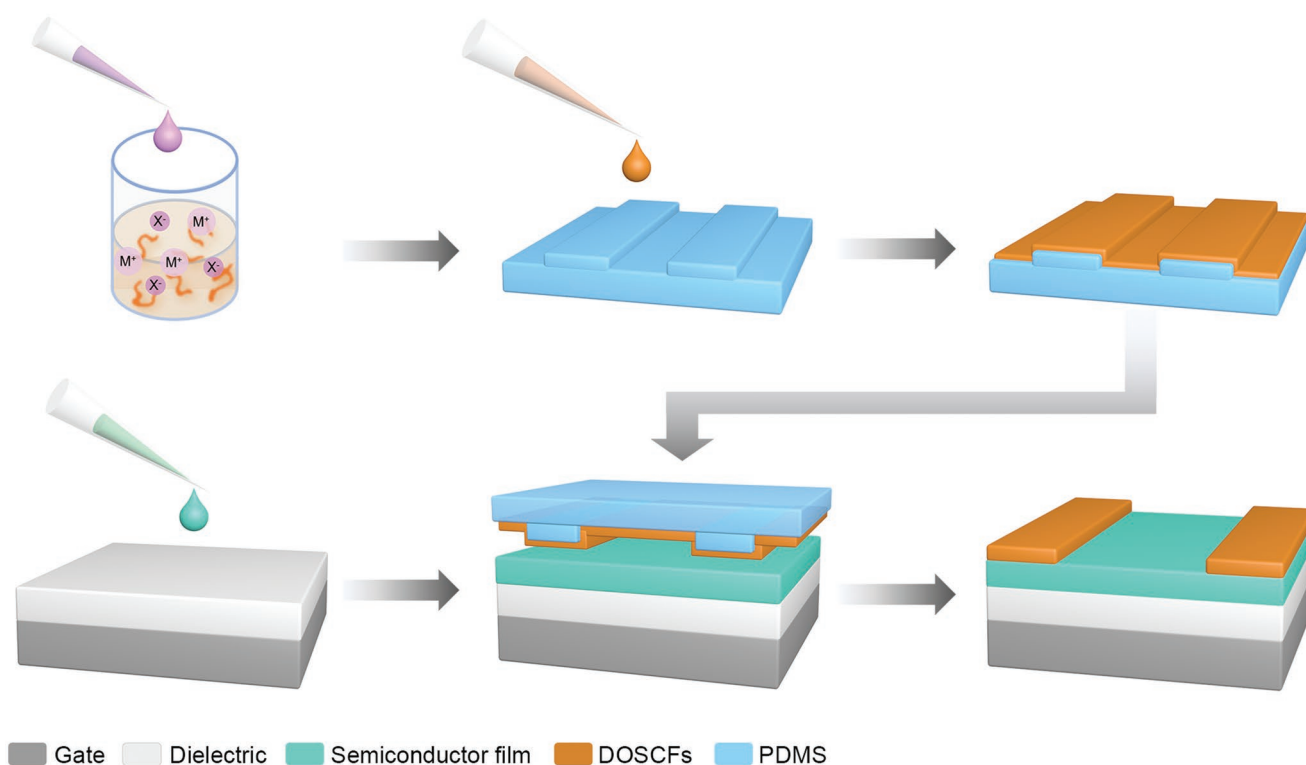
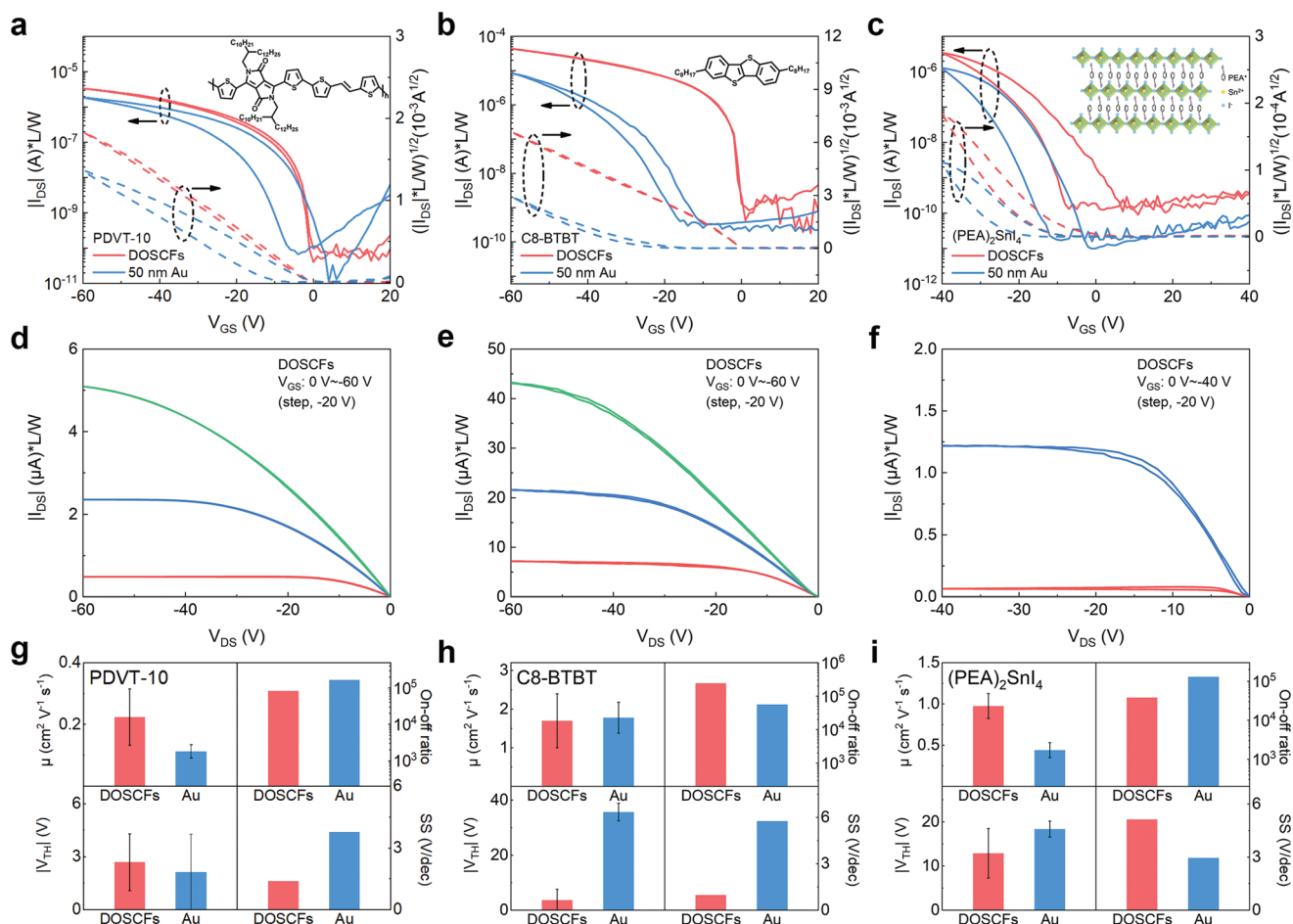


Figure 2. Schematic illustration of the usage of DOSCFs as vdW electrodes for FETs through PDMS stamping transfer method.



**Figure 3.** Fabrication and Characterization of FETs with DOSCFs as vdW electrodes. The transfer characteristics of FETs using Au and DOSCFs electrode (40 mol% TrTPFB) (measured at  $V_{DS} = -60$  V), with the chemical structure of the semiconductor shown in the insert: a) PDVT-10; b) C8-BTBT; and c)  $(\text{PEA})_2\text{SnI}_4$ . The output curves of FETs with DOSCFs: d) PDVT-10; e) C8-BTBT; and f)  $(\text{PEA})_2\text{SnI}_4$ . The summary of the electrical parameters for FETs with DOSCFs and Au electrodes: g) PDVT-10; h) C8-BTBT; and i)  $(\text{PEA})_2\text{SnI}_4$ . The parameter values are the average value of six devices and the error bars represent the standard deviation of six devices.

damage the lattice structure of C8-BTBT crystals. As a comparison, the transfer and output characteristics of the DOSCF devices are shown in Figure 3b,e, respectively. It is apparent that the DOSCF devices have much higher performance compared to the Au-electrode control devices by exhibiting much smaller  $V_{TH}$  ( $-3.64$  V) and lower SS ( $1.51$  V  $\text{dec}^{-1}$ ), which can be ascribed to the lowered Schottky barrier and reduced interface traps at the electrode/semiconductor interface. According to these results, we conclude that DOSCFs not only can be used as electrodes for p-channel devices, but also may help enhance the device performance due to its high work function and the formation of vdW contacts with perfect electrode/semiconductor interface.

Besides OFETs, we also attempted to use the PBTT-2T DOSCFs as electrodes for 2D layered perovskite  $(\text{PEA})_2\text{SnI}_4$  FETs. The preparation of  $(\text{PEA})_2\text{SnI}_4$  films was described in the experimental section, and the procedures for transferring DOSCF electrodes are the same as shown above.<sup>[23,32]</sup> It turns out that the DOSCF device shows an average mobility of  $0.97$   $\text{cm}^2$   $\text{V}^{-1}$   $\text{s}^{-1}$ , which is far higher than that of the control device with evaporated Au film as electrodes (average mobility

of  $0.44$   $\text{cm}^2$   $\text{V}^{-1}$   $\text{s}^{-1}$ ). This is possibly because the evaporation of Au causes damages to the perovskite lattice or results in chemical interaction, while the vdW contacts made by DOSCFs avoid such problems.<sup>[33–35]</sup> These results not only demonstrate the generality of using DOSCFs as electrodes for various semiconductors, but also suggest the superiority of them as electrodes.

Importantly, it should be mentioned that although here we have only shown doping PBTT-2T films to obtain DOSCFs as electrodes for p-type FETs, the strategy of doping OSCs for DOSCFs as electrodes is indeed a generally effective strategy as long as the DOSCFs satisfy the requirements mentioned above. As an example, we also have employed doped PBTTT- $\text{C}_{14}$  films by TrTPFB as electrodes for PDVT-10 FETs. The doped PBTTT- $\text{C}_{14}$  films show the highest  $\sigma$  of  $22.3$   $\text{S cm}^{-1}$  at a doping concentration of 40 mol%, and the corresponding PDVT-10 FETs exhibit very comparable performance to Au-electrode devices (Figure S9, Supporting Information). More than that, n-doped OSC films can also be employed as electrodes for n-type devices. For instance, we n-doped the polymer semiconductor PDCT with N-DMBI and obtained  $\sigma$  of  $2.1$   $\text{S cm}^{-1}$  at doping ratio of 60 wt%.<sup>[36]</sup> The PDCT FETs fabricated with doped PDCT films

operate well as n-type transistors (Figure S10, Supporting Information). We believe that with the development of more efficient n-dopants and/or semiconductors, more n-doped OSC films with high conductivity will be available for electrodes of n-type devices.<sup>[37–39]</sup> All these results demonstrate that the strategy of using DOSCFs as electrodes is not limited to a specific or a few OSCs, but universally applicable.

### 2.3. Unique Optical Advantages of DOSCFs as vdW Electrodes for photodetectors (PDs)

We note that DOSCFs are not only conductive enough to be electrodes, but also possess photo-absorption/transmittance properties, which are not observed in metal electrodes. In fact,

the PBBT-2T DOSCFs are found to exhibit 48.1% transparency while the Ag films show transparency of 0.7% under 450 nm illumination when their thicknesses are  $\approx 90$  nm (Figure 4a,b). Such semi-transparent property is for sure attractive for optoelectronics devices which usually need the transmittance of light. Here we showcase the utilization of the PBBT-2T DOSCFs as electrodes in organic PDs (OPDs). OPDs were fabricated on ITO substrates with blended P3HT:PC<sub>61</sub>BM bulk heterojunctions as active layers, as shown in Figure 4c. SnO<sub>2</sub> and P3HT/MoO<sub>3</sub> were used as the hole blocking layer and electron blocking layer, respectively, and the DOSCFs were used as the top-contact electrodes. The energy level alignment of the photodetector is illustrated in Figure 4d, which indicates that holes and electrons will be collected by the DOSCF and ITO electrodes, respectively. The absorption spectra of the P3HT:

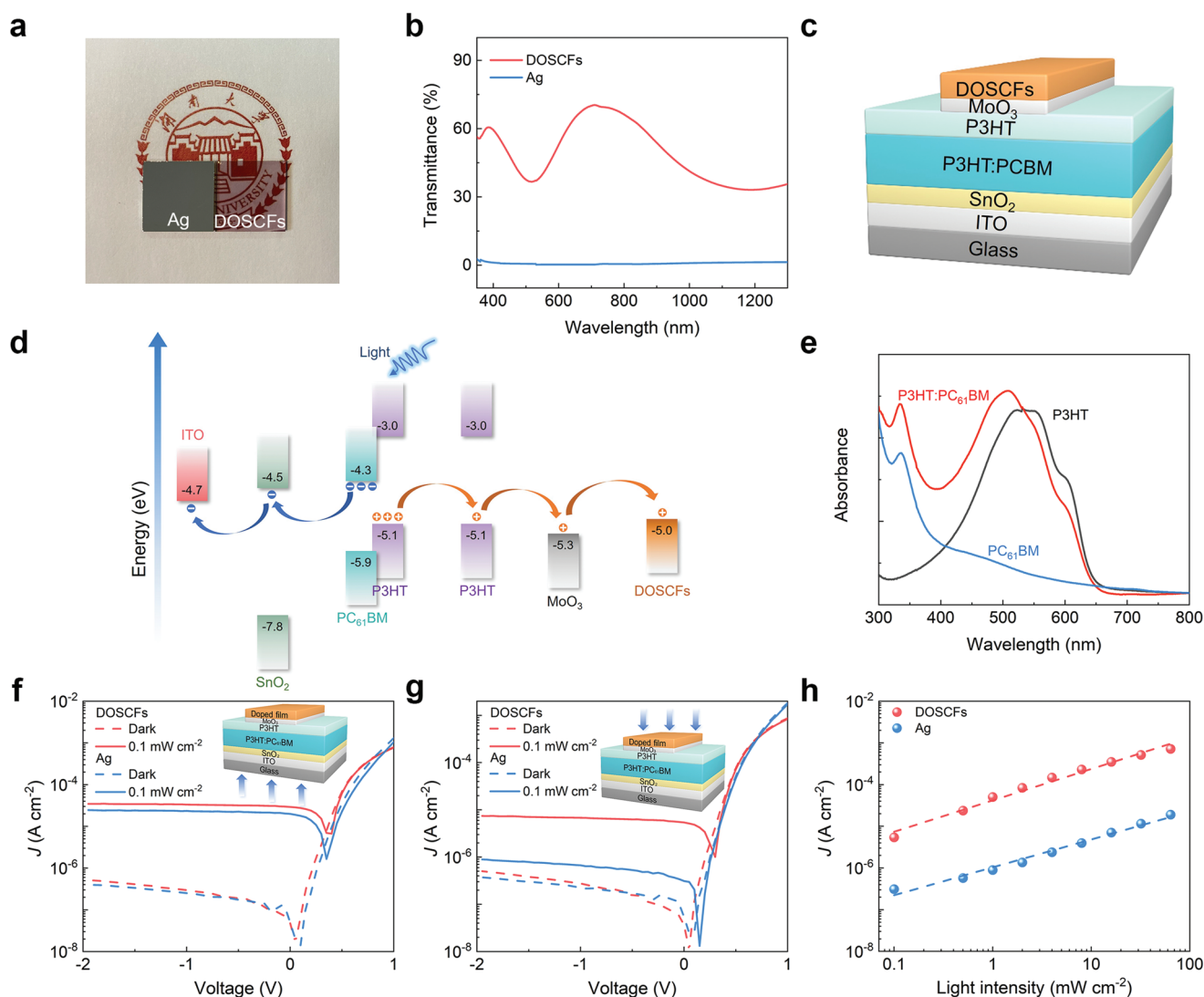


**Figure 4.** Characterization of the PDs with DOSCFs as vdW electrodes. a) Photographs of the PBBT-2T DOSCFs and Ag films, whose film thickness are  $\approx 90$  nm. b) Transmittance of the DOSCF electrodes and Ag electrodes. c) Structure of the photodetector device. d) Energy level diagram of the device. e) The absorption spectra of pristine P3HT film, PC<sub>61</sub>BM film and P3HT:PC<sub>61</sub>BM film. f) Current density versus voltage ( $J$ - $V$ ) curve of the photodetector in the dark and light ( $\lambda = 450$  nm, with illumination intensity of  $0.1 \text{ mW cm}^{-2}$ ) when light was illuminated from the ITO side. g) Current-voltage characteristics and h) the photocurrents as a function of illumination intensity at 0 V for the devices with light illuminated from the top-contact electrode (DOSCFs or Ag) side.

PC<sub>61</sub>BM layer is presented in Figure 4e, which shows strong absorption in the range of 300–650 nm.

To evaluate the photoelectric property of the photodetector, the  $J$ – $V$  curves of the devices under dark and illumination conditions (450 nm light irradiated from ITO side) were measured. As shown in Figure 4f, the device shows a typical rectifying behavior and obvious photo-response. With illumination intensity of 0.1 mW cm<sup>-2</sup>, the responsivity ( $R$ ) and detectivity ( $D^*$ ) of the device were estimated to be 0.29 A W<sup>-1</sup> and  $1.2 \times 10^{12}$  Jones at  $V = 0$  V, respectively (see Figure S12–S14, Supporting Information). Such device performance is very comparable to the reference device with Ag film as the top-contact electrode, just as seen in the  $J$ – $V$  curves (Figure 4f).

Interestingly, when the light was illuminated from the top-contact side, the DOSCF device shows much stronger photo-response compared to the reference device with Ag electrode, as shown in Figure 4g,h. The photocurrents of the DOSCF device are nearly one order of magnitude higher than those of the reference device in a wide range of illumination intensity (Figure 4h), which is attributed to the much higher transmittance of the PBBT-2T DOSCFs than metal films. Notably, the DOSCFs not only allow the transmission of light, but also can absorb light as seen in Figure 1d. Such special optical properties of DOSCFs bring them unique advantages not only in PDs, but also in solar cells.

#### 2.4. All-Organic FETs with High Flexibility Enabled by DOSCF Electrodes

In this section, we show the mechanical flexibility of the PBBT-2T DOSCFs and demonstrate the prototype device composed

of polymer substrates, polymer electrodes, polymer dielectric, and polymer semiconductor layer, which we name as the “all-organic FETs” or “true OFETs”.

First, the mechanical properties of the PBBT-2T DOSCFs were evaluated. For such purposes, the DOSCFs were deposited on pretreated PDMS substrates with foldable microscale structures as illustrated in Figure 5a.<sup>[40]</sup> The electrical performance of the DOSCFs was recorded when they were gradually stretched with strain varying from 0 to 65%. As seen in the current–voltage curves (Figure 5b) and analysis of the resistance (Figure 5c), the DOSCFs show little variation when the strain is less than 50%. Apart from the stretching test, the DOSCFs were used as conductive wires to connect a blue LED light, whose brightness remained almost unchanged when the DOSCFs were twisted or stretched (Figure 5d). These results indicate the feasibility of using DOSCFs as electrodes for flexible/stretchable devices.

Then, we were motivated to construct the “all-organic FETs” because most organic semiconductor devices in fact use metal films for electrodes, which is kind of a deviation from true “organic electronics”. To realize all-organic FETs, we first deposited the PBBT-2T DOSCFs on PEN substrates as gate electrodes, and then spin-coated Cytop layer as the dielectric. Following that, we used the PDMS stamping transfer method to assemble source/drain electrodes (PBBT-2T DOSCFs) and semiconductor layers to obtain bottom-gate bottom-contact (BGBC) devices as illustrated in Figure 6a (see Figure S16, Supporting Information). Figure 6b,c show the transfer and output characteristics of the all-organic FETs with PDVT-10 as the semiconductor layer, respectively. The devices exhibited beautiful transistor characteristics with negligible hysteresis. More than that, these devices were observed to possess

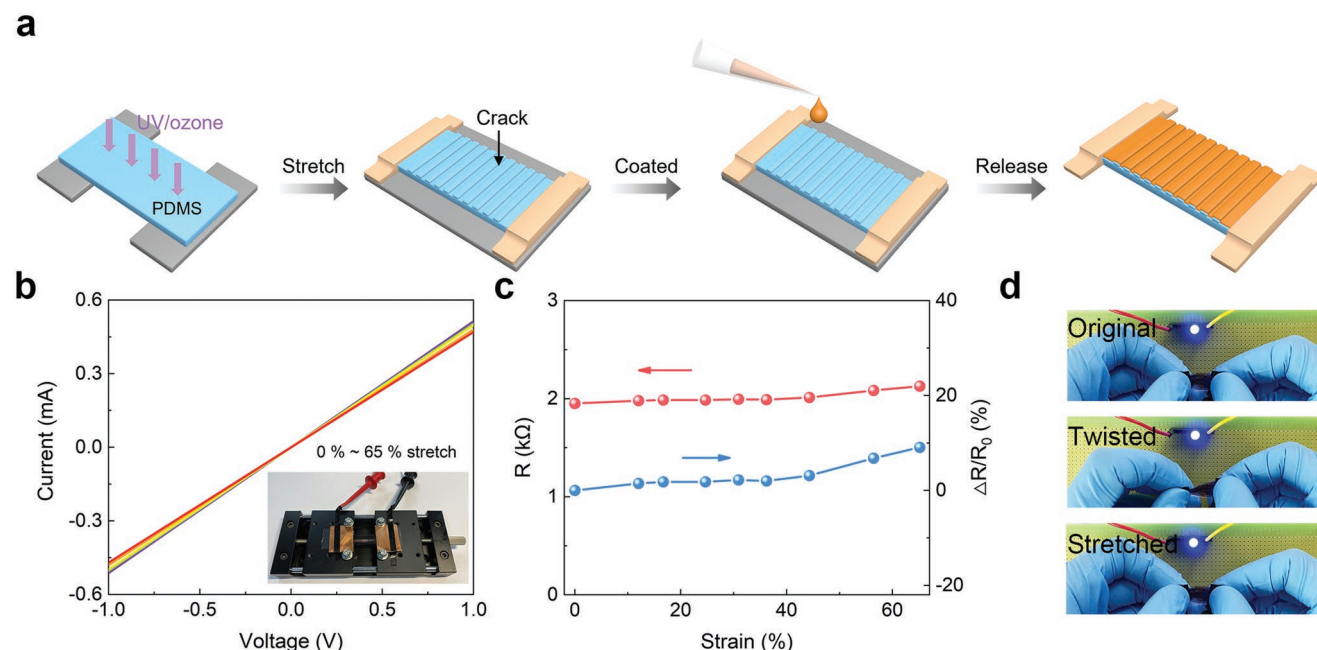


**Figure 5.** Characterization of the mechanical property of DOSCFs. a) Schematic diagram of the fabrication process of DOSCFs on stretchable substrates. b) The current–voltage curves of stretched PBBT-2T DOSCFs in the 0–65% stretching range (the setup for stretching test is shown in the inset). c) The dependence of resistance on stretching strain for the PBBT-2T DOSCFs. d) The brightness of the blue LED light connected by the PBBT-2T DOSCF electrodes under different states (top: original, middle: twisted, bottom: stretched).

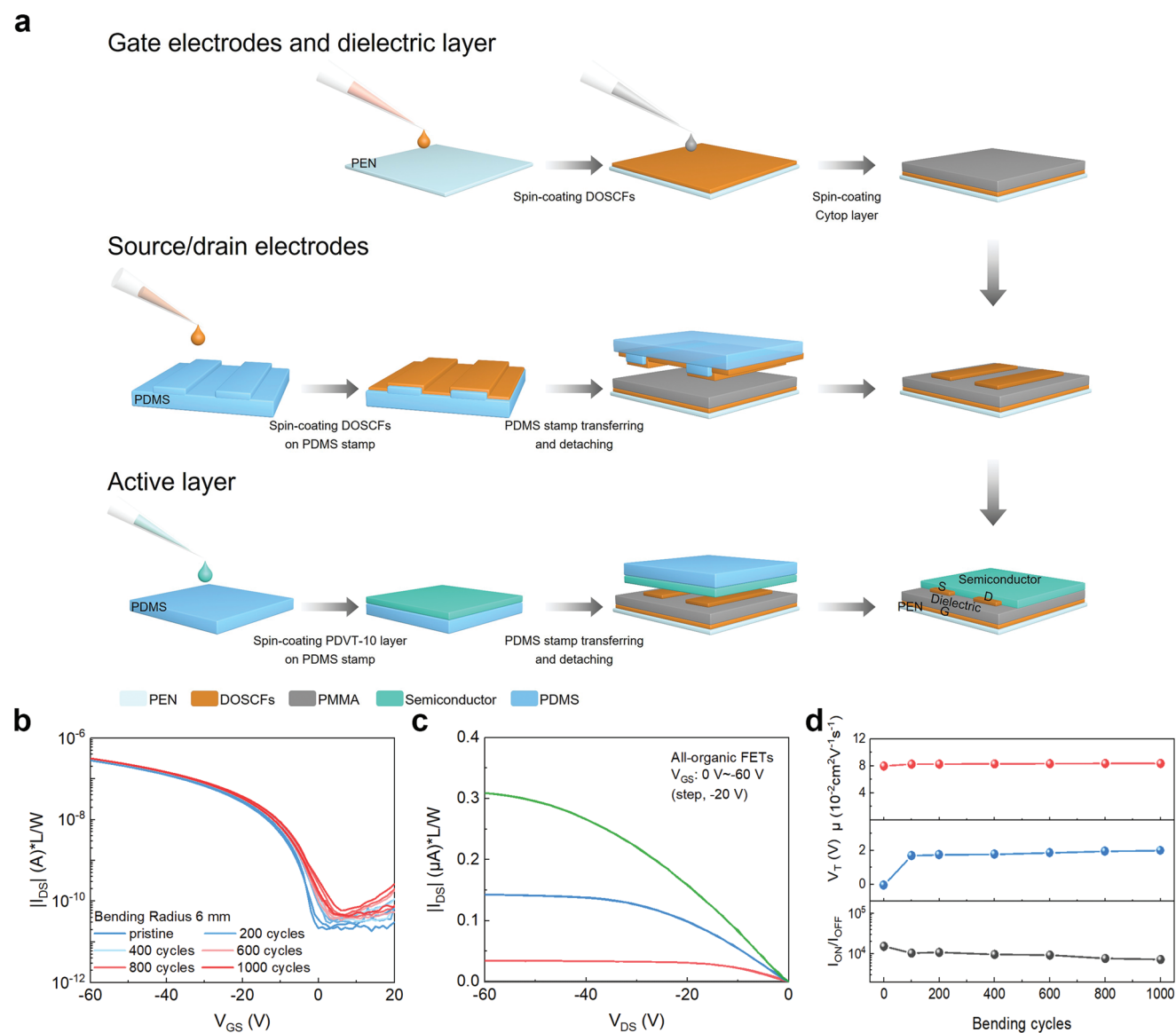


**Figure 6.** Fabrication and characterization of all-organic FETs with DOSCF electrodes. a) Schematic diagram of the fabrication process of all-organic FETs; b) the variation of transfer curve of all-organic FETs during bending cycles with bending radius of 6 mm; c) output curve of all-organic FETs at pristine state; d) the variation of hole mobility, threshold voltage, and  $I_{ON}/I_{OFF}$  ratio as a function of the bending cycles.

excellent mechanical flexibility. As presented in Figure 6d which shows the variation of hole mobility,  $I_{ON}/I_{OFF}$  ratio and threshold voltage versus the bending cycles, one can see that the electrical properties of the all-organic FETs were maintained without significant changes even after being bended over 1000 cycles at bending radius of 6 mm. These results indicate DOSCFs are promising candidates for electrodes of flexible/stretchable devices.

### 3. Conclusion

In summary, we demonstrate the feasibility of doping OSC films to obtain DOSCF electrodes for semiconductor devices and show their advantages over metal electrodes in devices. By

selection of proper OSCs and dopants, the DOSCFs can be sufficiently conductive as well as uniform, and thus appropriate for electrode usages. We employed the PDMS stamping transfer method to integrate the DOSCFs with various semiconductors to form vdW contacts for semiconductor devices. Owing to the unique advantages of DOSCFs such as semi-transparency and mechanical flexibility/stretchability, the devices show remarkable performance or properties that are not available in metal-electrode devices. The DOSCFs also enable the construction of proof-of-concept devices: all-organic FETs. Overall, the methodology of doping OSC films for electrodes of semiconductor devices is viable, and can be applied to different OSCs and dopants. This study may open up plenty of opportunities to construct interesting and novel devices by the usage of DOSCFs.



## 4. Experimental Section

**Preparation of OSC Solutions and Doped Solutions:** TrTPFB (purchased from Strem Chemicals, Inc.) and PBTT-2T were dissolved in chlorobenzene (purchased from Sigma Aldrich, Inc.) to form solutions at concentration of 20 and 5 g L<sup>-1</sup>, respectively. Similarly, poly[2,5-bis(2decyltetradecyl)pyrrolo[3,4-c]pyrrole-1,4(2H,5H)-dione-alt-5,5"di(thiophen-2-yl)-2,2"-(E)-2-(2-(thiophen-2-yl)vinyl)thiophene] PDVT-10, poly(3-hexylthiophene) P3HT, Poly(2,5-bis(3-tetradecylthiophen-2-yl)thieno[3,2-b]thiophene) (PBTTT-C<sub>14</sub>), PDCT, and N-DMBI were dissolved in chlorobenzene (CB) at concentration of 5 g L<sup>-1</sup>, 5 g L<sup>-1</sup>, 10 g L<sup>-1</sup>, 3 g L<sup>-1</sup>, and 5 g L<sup>-1</sup>, respectively. Notably, PBTT-2T solutions need to be pre-heated at 60 °C for 2 h before usage, PBTTT-C<sub>14</sub> solution was heated at 80 °C for 1 h, and PDCT solution was heated at 120 °C for 1 h. Then, the dopants and PBTT-2T solutions were mixed according to the desired doping ratio for use.

**Preparation of Perovskite Solutions:** PEAI and SnI<sub>2</sub> with a molar ratio of 2:1 was added to a mixture of DMF and NMP with a volume ratio of 3:1 to form 0.1 M (PEAI)<sub>2</sub>SnI<sub>4</sub> precursor solutions. The precursor solutions were heated at 60 °C for 6 h. Then, the precursor solutions were filtered through 0.45 μm polytetrafluoroethylene (PTFE) filters and cooled down to room temperature naturally.

**UV-Vis-NIR and ESR Measurements:** The ultraviolet-visible-near-infrared (UV-vis-NIR) absorption spectra of doped solution samples were carried out with UV-3600PLUS (SHIMADZU). The electron spin resonance (ESR) was measured on a JEOL JES-FA200 ESR spectrometer at room temperature. In ESR measurements, samples were prepared by spin-coating onto a glass substrate and then placed in paramagnetic tubes.

**Conductivity and KPM Measurements:** For electrical conductivity measurements, a four-point probe method was used. In this method, Si<sup>++</sup>/SiO<sub>2</sub> substrates with predefined electrodes (Cr/Au: 3 nm/35 nm) by photolithography and thermal evaporation, sequentially. Before being used, the substrates first were cleaned sequentially with deionized water, acetone, isopropanol, and dry with Argon gas. The substrates were then treated with UV/ozone for 15 min. The doped solutions were spin-coated to form a thin film on the substrate at a speed of 1500 rpm for 30 s and annealed at 100 °C for 10 mins in the glovebox, and then the devices were measured through a Keithley 4200 semiconductor analyzer. For work functions measurements, the doped films were deposited on the Si<sup>++</sup>/SiO<sub>2</sub> substrate and measured on a Kelvin probe (KP020).

**AFM and Optical Microscope Measurements:** The optical images were inspected by optical microscope (Olympus BX53M). The AFM characterizations were performed through an atomic force microscope (AFM, Bruker Dimension Icon) system.

**PDMS Stamping Transfer Method:** The PDMS precursor (Sylgard 184, Dow Corning) were prepared by a mixture of the elastomer and curing agent (10:1 weight ratio). The mixed solution was stirred thoroughly with a magnetic stir for 10 mins, and then the mixed prepolymer solutions were directly cast on top of the mold, evacuated for 20 min to remove any air bubbles. Following that the mixture was placed in a vacuum drying oven and heated at 80 °C for 180 min. After curing, the PDMS stamps were removed from the mold and cut into shapes of appropriate dimensions. Before being used, the PDMS stamp was dipped in CB for 5 min, followed by ultrasonic cleaning in isopropyl alcohol (IPA) for 1 min. The washing process modifies the surface energy of PDMS stamps, which allows the easy deposition of DOSCFs on the surface of the stamps. The DOSCFs were spin-coated on PDMS stamps at a speed of 1000 rpm for 20 s, and then the DOSCFs on the PDMS stamps was placed on the top of semiconductor layer. By applying slightly external force, the DOSCFs was completely transferred, after which the PDMS substrate was peeled off to complete the transfer process.

**Fabrication and Characterization of FETs:** For BGTC FETs, the Si<sup>++</sup>/SiO<sub>2</sub> substrates were first cleaned following the above-mentioned method. The OSC solutions were spin-coated on the OTS-treated Si<sup>++</sup>/SiO<sub>2</sub> substrates at a speed of 1500 rpm for 30 s

and then annealed (PDVT-10: 180 °C for 5 mins; P3HT: 130 °C for 5 mins; PBTT-2T: 100 °C for 10 mins; PDCT: 150 °C for 10 mins). (PEAI)<sub>2</sub>SnI<sub>4</sub>perovskite films were made by spin-coating solutions at 4000 rpm for 30 s on bare Si<sup>++</sup>/SiO<sub>2</sub> substrates and then annealing at 100 °C for 10 min. For DOSCF-electrode FETs, source and drain electrodes (PBTT-2T films doped by 40 mol% TrTPFB) were fabricated using the PDMS stamping transfer method. The corresponding Au-electrode FETs were fabricated all the procedures being the same except that gold electrodes were deposited by thermal evaporation through a shadow mask that defined channel length (150 μm) and width (1000 μm). Electrical characteristics of all OFETs were recorded using an Agilent B2912A source meter. All these processes were carried out in a glovebox with inert argon ambient.

**Solvent Vapor Annealing Growth of C8-BTBT:** C8-BTBT and PMMA were dissolved in CB (20 g L<sup>-1</sup>) and mixed in the volume ratio 1:1. The mixed solution were spin-coated at 2000 rpm for 40 s onto Si<sup>++</sup>/SiO<sub>2</sub> substrates. Then, the substrates were attached to the top of the petri dish filled with chloroform at room temperature for 1 h. Finally, single crystals were obtained by heated at 70 °C for 1 h to remove any residues.

**Fabrication of Photodetectors:** The ITO substrates were ultrasonically cleaned in deionized water, acetone, deionized water, and isopropyl alcohol each for 15 min, and blown dry by nitrogen gas, and further treated by UV/ozone for 15 min. SnO<sub>2</sub> was spin-coated on ITO at 3000 rpm for 30 s, and annealed in air at 150 °C for 30 min. A solution of P3HT and PC<sub>61</sub>BM blend (1:1) dissolved in chlorobenzene at 20 g L<sup>-1</sup> concentration was heated at 50 °C for 8 h. Next, the blend solution was spin-coated on the substrate at 1000 rpm for 60 s. Subsequently, P3HT (10 g L<sup>-1</sup>) films was transferred using PDMS stamping transfer method and MoO<sub>3</sub> layer (40 nm) was thermally evaporated at 2 Å s<sup>-1</sup>. Finally, DOSCF electrodes were transferred on top of MoO<sub>3</sub> using PDMS stamps. For control devices, Ag (100 nm) as the electrode was thermally evaporated at 0.2 Å s<sup>-1</sup>.

**Fabrication of All-Organic FETs:** The BGBC device configuration was adopted for such devices. The gate electrode (PBTT-2T DOSCFs) was spin-coated onto PEN substrates at 1000 rpm for 20 s, and annealed at 100 °C for 10 min. Sequentially, the Cytop solution (3:1) was dropped and then spin-coated at 1000 rpm for 30 s, and annealed at 90 °C for 20 min. The PDMS stamping transfer method was used to fabricate S/D electrodes (PBTT-2T DOSCFs). Finally, the semiconductor film (PDVT-10 films) was deposited atop by the PDMS stamping transfer method.

**Statistical Analysis:** The performance data of the FETs shown in Figure 3 were obtain from 6 devices for each kind of FETs. The mean represents the average value of the 6 devices and the error bar represents the standard deviation of the 6 devices. The data processing was performed by Origin software.

## Supporting Information

Supporting Information is available from the Wiley Online Library or from the author.

## Acknowledgements

Y. H. thanks the National Key Research and Development Program (2022YFB3603802; 2021YFA1200700), the National Natural Science Foundation of China (62222403; 62074054; U21A20497; 22275157), Natural Science Foundation of Hunan Province (2022JJ10019; 2019GK2245; 2020JJ1002), and Shenzhen Science and Technology Innovation Commission (RCYX20200714114537036) for financial support.

## Conflict of Interest

The authors declare no conflict of interest.

## Data Availability Statement

The data that support the findings of this study are available from the corresponding author upon reasonable request.

## Keywords

doping, field-effect transistors, organic semiconductors, photodetectors, van der Waals electrodes

Received: December 15, 2022

Revised: March 3, 2023

Published online: March 22, 2023

- [1] Z. Qin, H. Gao, H. Dong, W. Hu, *Adv. Mater.* **2021**, *33*, 2007149.
- [2] H. Ren, J.-D. Chen, Y.-Q. Li, J.-X. Tang, *Adv. Sci.* **2021**, *8*, 2002418.
- [3] S. Wang, L. Peng, H. Sun, W. Huang, *J Mater Chem* **2022**, *10*, 12468.
- [4] J. Y. Kim, J.-W. Lee, H. S. Jung, H. Shin, N.-G. Park, *Chem. Rev.* **2020**, *120*, 7867.
- [5] H. Kleemann, K. Krechan, A. Fischer, K. Leo, *Adv. Funct. Mater.* **2020**, *30*, 1907113.
- [6] Y. Qian, X. Zhang, L. Xie, D. Qi, B. K. Chandran, X. Chen, W. Huang, *Adv. Mater.* **2016**, *28*, 9243.
- [7] T. C. Shyu, P. F. Damasceno, P. M. Dodd, A. Lamoureux, L. Xu, M. Shlian, M. Shtein, S. C. Glotzer, N. A. Kotov, *Nat. Mater.* **2015**, *14*, 785.
- [8] D. S. Gray, J. Tien, C. S. Chen, *Adv. Mater.* **2004**, *16*, 393.
- [9] D.-Y. Khang, H. Jiang, Y. Huang, J. A. Rogers, *Science* **2006**, *311*, 208.
- [10] J. A. Fan, W.-H. Yeo, Y. Su, Y. Hattori, W. Lee, S.-Y. Jung, Y. Zhang, Z. Liu, H. Cheng, L. Falgout, M. Bajema, T. Coleman, D. Gregoire, R. J. Larsen, Y. Huang, J. A. Rogers, *Nat. Commun.* **2014**, *5*, 3266.
- [11] R.-H. Kim, D.-H. Kim, J. Xiao, B. H. Kim, S.-I. Park, B. Panilaitis, R. Ghaffari, J. Yao, M. Li, Z. Liu, V. Malyarchuk, D. G. Kim, A.-P. Le, R. G. Nuzzo, D. L. Kaplan, F. G. Omenetto, Y. Huang, Z. Kang, J. A. Rogers, *Nat. Mater.* **2010**, *9*, 929.
- [12] Z. Wei, Y. Tong, P. Zhao, X. Zhao, Q. Tang, Y. Liu, *Appl. Surf. Sci.* **2019**, *480*, 523.
- [13] Y. Gao, Y. Shao, L. Yan, H. Li, Y. Su, H. Meng, X. Wang, *Adv. Funct. Mater.* **2016**, *26*, 4456.
- [14] C. Wang, H. Dong, L. Jiang, W. Hu, *Chem. Soc. Rev.* **2018**, *47*, 422.
- [15] S. Wang, Z. Wang, Y. Huang, Y. Hu, L. Yuan, S. Guo, L. Zheng, M. Chen, C. Yang, Y. Zheng, J. Qi, L. Yu, H. Li, W. Wang, D. Ji, X. Chen, J. Li, L. Li, W. Hu, *ACS Appl Mater Interfaces* **2021**, *13*, 17852.
- [16] E. Dauzon, Y. Lin, H. Faber, E. Yengel, X. Sallenave, C. Plesse, F. Goubard, A. Amassian, T. D. Anthopoulos, *Adv. Funct. Mater.* **2020**, *30*, 2001251.
- [17] E. Dauzon, A. E. Mansour, M. R. Niazi, R. Munir, D. M. Smilgies, X. Sallenave, C. Plesse, F. Goubard, A. Amassian, *ACS Appl Mater Interfaces* **2019**, *11*, 17570.
- [18] J. Rivnay, R. M. Owens, G. G. Malliaras, *Chem. Mater.* **2014**, *26*, 679.
- [19] K. Feron, R. Lim, C. Sherwood, A. Keynes, A. Brichta, P. Dastoor, *Int. J. Mol. Sci.* **2018**, *19*, 2382.
- [20] Y. Zhong, V. Untilova, D. Muller, S. Guchait, C. Kiefer, L. Herrmann, N. Zimmermann, M. Brosset, T. Heiser, M. Brinkmann, *Adv. Funct. Mater.* **2022**, *32*, 2202075.
- [21] H. Guo, C.-Y. Yang, X. Zhang, A. Motta, K. Feng, Y. Xia, Y. Shi, Z. Wu, K. Yang, J. Chen, Q. Liao, Y. Tang, H. Sun, H. Y. Woo, S. Fabiano, A. Facchetti, X. Guo, *Nature* **2021**, *599*, 67.
- [22] I. E. Jacobs, Y. Lin, Y. Huang, X. Ren, D. Simatos, C. Chen, D. Tjhe, M. Statz, L. Lai, P. A. Finn, W. G. Neal, G. D'avino, V. Lemaury, S. Fratini, D. Beljonne, J. Strzalka, C. B. Nielsen, S. Barlow, S. R. Marder, I. McCulloch, H. Sirringhaus, *Adv. Mater.* **2022**, *34*, 2102988.
- [23] J. Guo, Y. Liu, P.-A. Chen, X. Qiu, H. Wei, J. Xia, H. Chen, Z. Zeng, L. Liao, Y. Hu, *Adv. Electron. Mater.* **2022**, *8*, 2200148.
- [24] Y. Hu, Z. D. Rengert, C. Mcdowell, M. J. Ford, M. Wang, A. Karki, A. T. Lill, G. C. Bazan, T.-Q. Nguyen, *ACS Nano* **2018**, *12*, 3938.
- [25] J. Guo, G. Li, H. Reith, L. Jiang, M. Wang, Y. Li, X. Wang, Z. Zeng, H. Zhao, X. Lu, G. Schierning, K. Nielsch, L. Liao, Y. Hu, *Adv. Electron. Mater.* **2020**, *6*, 1900945.
- [26] J. Guo, Y. Liu, P.-A. Chen, X. Wang, Y. Wang, J. Guo, X. Qiu, Z. Zeng, L. Jiang, Y. Yi, S. Watanabe, L. Liao, Y. Bai, T.-Q. Nguyen, Y. Hu, *Adv. Sci.* **2022**, *9*, 2203111.
- [27] Y. Chen, L. Zhao, P.-A. Chen, Y. Li, J. Guo, Y. Liu, X. Qiu, J. Xia, K. Chen, H. Chen, X. Lu, L. Jiang, L. Liao, T.-Q. Nguyen, Y. Hu, *Matter* **2022**, *5*, 2882.
- [28] J. Mai, N. Tang, W. He, Z. Zou, C. Luo, A. Zhang, Z. Fan, S. Wu, M. Zeng, J. Gao, G. Zhou, X. Lu, J.-M. Liu, *Nanoscale Res. Lett.* **2019**, *14*, 169.
- [29] H. Xia, S. Tong, C. Zhang, C. Wang, J. Sun, J. He, J. Zhang, Y. Gao, J. Yang, *Appl. Phys. Lett.* **2018**, *112*, 233301.
- [30] C. Liu, T. Minari, X. Lu, A. Kumatani, K. Takimiya, K. Tsukagoshi, *Adv. Mater.* **2011**, *23*, 523.
- [31] S. - G. Yu, Y. - R. Jo, M. - W. Kim, B. - J Kim, *J Phys Chem* **2020**, *124*, 14873.
- [32] Y. Liu, P.-A. Chen, X. Qiu, J. Guo, J. Xia, H. Wei, H. Xie, S. Hou, M. He, X. Wang, Z. Zeng, L. Jiang, L. Liao, Y. Hu, *iScience* **2022**, *25*, 104109.
- [33] J. Wang, S. P. Senanayak, J. Liu, Y. Hu, Y. Shi, Z. Li, C. Zhang, B. Yang, L. Jiang, D. Di, A. V. Ievlev, O. S. Ovchinnikova, T. Ding, H. Deng, L. Tang, Y. Guo, J. Wang, K. Xiao, D. Venkateshvaran, L. Jiang, D. Zhu, H. Sirringhaus, *Adv. Mater.* **2019**, *31*, 1902618.
- [34] F. Liu, L. Wang, J. Wang, F. Wang, Y. Chen, S. Zhang, H. Sun, J. Liu, G. Wang, Y. Hu, C. Jiang, *Adv. Funct. Mater.* **2021**, *31*, 2005662.
- [35] X. Qiu, Y. Liu, J. Xia, J. Guo, P.-A. Chen, H. Wei, J. Guo, X. Shi, C. Chen, Z. Zeng, H. Chen, L. Jiang, L. Liao, Y. Hu, *Cell Rep. Phys. Sci.* **2023**, *4*, 101217.
- [36] M. Xiong, X. Yan, J.-T. Li, S. Zhang, Z. Cao, N. Prine, Y. Lu, J.-Y. Wang, X. Gu, T. Lei, *Angew. Chem., Int. Ed.* **2021**, *60*, 8189.
- [37] C.-Y. Yang, Y.-F. Ding, D. Huang, J. Wang, Z.-F. Yao, C.-X. Huang, Y. Lu, H.-I. Un, F.-D. Zhuang, J.-H. Dou, C.-A. Di, D. Zhu, J.-Y. Wang, T. Lei, J. Pei, *Nat. Commun.* **2020**, *11*, 3292.
- [38] H. Wei, P.-A. Chen, J. Guo, Y. Liu, X. Qiu, H. Chen, Z. Zeng, T.-Q. Nguyen, Y. Hu, *Adv. Funct. Mater.* **2021**, *31*, 2102768.
- [39] X. Yan, M. Xiong, X.-Y. Deng, K.-K. Liu, J.-T. Li, X.-Q. Wang, S. Zhang, N. Prine, Z. Zhang, W. Huang, Y. Wang, J.-Y. Wang, X. Gu, S. K. So, J. Zhu, T. Lei, *Nat. Commun.* **2021**, *12*, 5723.
- [40] Z. Tan, H. Li, Z. Niu, X. Chen, H. Yang, W. Lv, D. Ji, J. Li, L. Li, W. Hu, *J Mater Chem* **2021**, *9*, 4046.